PAPER

Si-thiol supported atomic-scale palladium as efficient and recyclable catalyst for Suzuki coupling reaction

To cite this article: Xiazhang Li et al 2020 Nanotechnology 31 355704

View the article online for updates and enhancements.



IOP ebooks™

Bringing together innovative digital publishing with leading authors from the global scientific community.

Start exploring the collection-download the first chapter of every title for free.

IOP Publishing Nanotechnology

Nanotechnology 31 (2020) 355704 (8pp)

https://doi.org/10.1088/1361-6528/ab9473

Si-thiol supported atomic-scale palladium as efficient and recyclable catalyst for Suzuki coupling reaction

Xiazhang Li^{1,2}, Zuo-Gang Huang², Haiguang Zhang¹, Yuying Zhang², Chunyan Zhang², Hui-Yin H Li^{2,3}, David C Martin² and Chaoying Ni^{2,4}

- Advanced Catalysis and Green Manufacturing Collaborative Innovation Center, Changzhou University, Changzhou 213164, People's Republic of China
- ² Department of Materials Science and Engineering, University of Delaware, Newark, DE 19716, United States of America

E-mail: cni@udel.edu

Received 8 March 2020, revised 28 April 2020 Accepted for publication 19 May 2020 Published 16 June 2020



Abstract

Atomic-scale catalysts leverage the advantages of both heterogeneous catalysts for their stability and reusability and homogeneous catalysts for their isolated active sites. Here, a palladium catalyst supported by Si-thiol, a commercially available mercaptopropyl-modified and TMS-passivated amorphous silica, was synthesized and characterized by SEM,TEM, aberration-corrected STEM-HAADF, XRD, FT-IR and XPS. Statistical analysis revealed that the catalytic Pd species predominantly consisted of intermediate sized nanoparticles (<2 nm), small amounts of essentially isolated atoms (ca. 0.1 nm), and limited amounts of somewhat larger nanoparticles (<5 nm). The nanoscale atomic clusters dominated the reactivity and served as the key active sites for Suzuki coupling. The outcomes of the reaction were greatly affected by the choice of solvents, and Pd/Si-thiol was demonstrated to be reusable for more than three times without a noticeable loss of catalytic activity.

$$R \longrightarrow Br + (HO)_2B \longrightarrow R' \xrightarrow{Pd/Si-Thiol} R \longrightarrow R'$$
base, solvent

Supplementary material for this article is available online

Keywords: atom clusters, palladium, Si-thiol, Suzuki reaction, recyclable catalyst, HRTEM

(Some figures may appear in colour only in the online journal)

1. Introduction

The Pd-catalyzed Suzuki coupling reactions have been widely used in modern synthesis [1]. However, the use of Pd in active pharmaceutical ingredients (APIs) could result in the possibility of Pd-containing impurities in the isolated products, and the post reaction removal of Pd is a challenging task [2]. To meet strict limits for heavy metal residues in APIs,

adsorption of the residual Pd to an appropriate solid scaffold followed by the removal of the absorbent with Pd by filtration from the process stream. However, the screening of adequate adsorbents is time-consuming and expensive [3]. One concept is to use Pd adsorbed on scavenger as a catalyst to minimize the Pd content in the product and increase the amount recovered in recycling. Crudden *et al* have developed a mesoporous silica modified with mercaptopropyl silyloxy groups (O₃Si(CH₂)₃SH) which can scavenge Pd to less than 1 ppb in reaction solutions [4, 5]. The material grabs Pd and holds onto it so well that it can in turn be used repeatedly as a catalyst

³ Wilmington PharmaTech Co., 229A Lake Drive, Newark, DE 19702, United States of America

Author to whom any correspondence should be addressed.

for Suzuki-Miyaura and Mizoroki-Heck coupling reactions, leaving as little as 3 ppb of Pd in solution. Validation tests showed that the catalytic activity of the new material occurred on the surface of the silica, rather than by the Pd dissociating out into solution.

Si-thiol is a commercially available scavenger that can remove a variety of transition metals. [6] It is based on mercaptopropyl-grafted amorphous silica gel and the residual silanols on its surface have been end-capped by trimethylsilyl moieties. This functionalized silica also has the advantages of containing a non-swelling backbone and being static-charge free which is convenient for handling [7]. Using an appropriate support material that strongly interacts with the metal species is expected to prevent aggregation, creating stable and finely dispersed metal clusters with a high catalytic activity, which benefits the recyclability and simplifies post-production purification.

Although there has been report of Suzuki coupling reactions catalyzed by Pd supported on thiol-functionalized mesoporous organosilica [8], the protocols for the mesostructured silicate synthesis and surface functionalization methods were different and would have dramatic influences on catalytic performances. In addition, those supported catalysts such as PVPy or COF loaded Pd are inhomogeneous and their size is usually in the nanoscale range since the surface free energy of metals increases significantly with the decrease of particle size and leads to the aggregation of small clusters [9, 10]. Such structural heterogeneities not only reduce the metal atom efficiency but also frequently lead to undesired side reactions. The nominal size, shape and surface of metal particles is therefore an important factor to determine when analyzing the performance of a particular catalyst [11]. In recent years, several efforts have been reported to develop state-of-the-art singleatom (Pt, Pd, Co, etc) catalysts [12]. The low-coordination and unsaturated atoms often function as active sites. Reducing the size of the particles to the atomic and near-atomic scale is highly desirable for catalytic reactions since the interaction of hydrogen or organic molecules with small Pd clusters is a strong function of the cluster size [13]. Atomic-scale Pd catalysis with scavenger for Suzuki reaction has been rarely reported. In the present work, a Pd/Si-thiol hybrid catalyst system was successfully prepared and its catalytic reactivity was investigated in a typical Suzuki coupling reaction in various solvents through a systematic optimization by monitoring the reaction kinetics.

2. Experimental

2.1. Catalyst preparation

0.90 mmol Pd(OAc)₂ was added to 20 ml of toluene, and stirred at 80 °C under N_2 flow for 15 min to obtain a clear solution. The solution was then cooled to room temperature and 1.8 mmol of Si-thiol was added before heating at 110 °C for 4 h. After cooling down to room temperature and stirring for 12 h, the mixture was filtered and washed with toluene (3 × 20 ml). A light brown powder was obtained after drying under vacuum at 40 °C for 12 h. The specific chemical reaction is shown in (equation 1)

2.2. Catalyst characterization

Powder x-ray diffraction (PXRD) was performed on a Rigaku x-ray diffractometer with Cu Kα radiation (Rigaku, D/max-RB). XPS analysis was carried out by an x-ray photoelectron spectrometer ESCA (Thermo Fisher Scientific, ESCALAB 250, Mono Al Kα source 1486.6 eV). FT-IR spectra of samples were obtained using a Nicolet 460 with diffuse reflectance sampling accessory at a resolution of 4 cm⁻¹. Measurements were performed on powders with KBr as diluents. SEM characterization was performed using a JSM-7400F field emission (FE) scanning electron microscope. Prior to SEM analysis, the solid samples were sprinkled onto adhesive carbon tapes supported on metallic stubs, and then coated with conductive gold or carbon. For TEM analysis, a sample of Pd/Si-thiol was dispersed in water. A drop of the dispersion was transferred onto a TEM Cu-grid and was allowed to dry in ambient environment. TEM characterization was performed using a JEM-2010F transmission election microscope at 200 kV. STEM-HAADF characterization was performed with a sub-angstrom resolution aberration-corrected FEI Titan 80-300 transmission election microscope operating at 300 kV.

2.3. Procedure for Suzuki coupling reaction

A mixture of *p*-BrPhOMe (85 μ l, 0.67 mmol), *p*-CF₃PhB(OH)₂ (0.80 mmol), K₂CO₃ (1.33 mmol) and *n*-PrOH (2.0 ml) was stirred under N₂ flow, followed by adding 12 mg of Pd/Si-thiol. The reaction was monitored by HPLC under heating at 85 °C for 3–24 h. After the reaction was completed, the product was purified by chromatography on silica gel and analyzed by ¹H NMR (400 MHz).

2.4. Procedure for catalyst recycling

A mixture of p-AcPhBr (10 mmol), p-CF₃PhB(OH)₂ (12 mmol), K_2 CO₃ (20 mmol) and n-PrOH (30 ml) was stirred under a N_2 atmosphere, followed by adding 0.10 mmol Pd/Sithiol. The reaction was monitored by HPLC under heating at 85 °C for 2 h. After the reaction was completed below 40 °C, the product was washed with 2 \times 10 ml of n-PrOH and analyzed by 1 H NMR (400 MHz). To recycle the catalyst, the solid cake was washed with 2 \times 20 ml water, 10 ml n-PrOH, and 10 ml toluene, and then dried under vacuum at room temperature for 12 h.

3. Results and discussion

3.1. Microstructure analysis

The morphology of Si-thiol matrix and Pd/Si-thiol catalyst is shown in figure 1. Figure 1(a) exhibits an FE-SEM image of

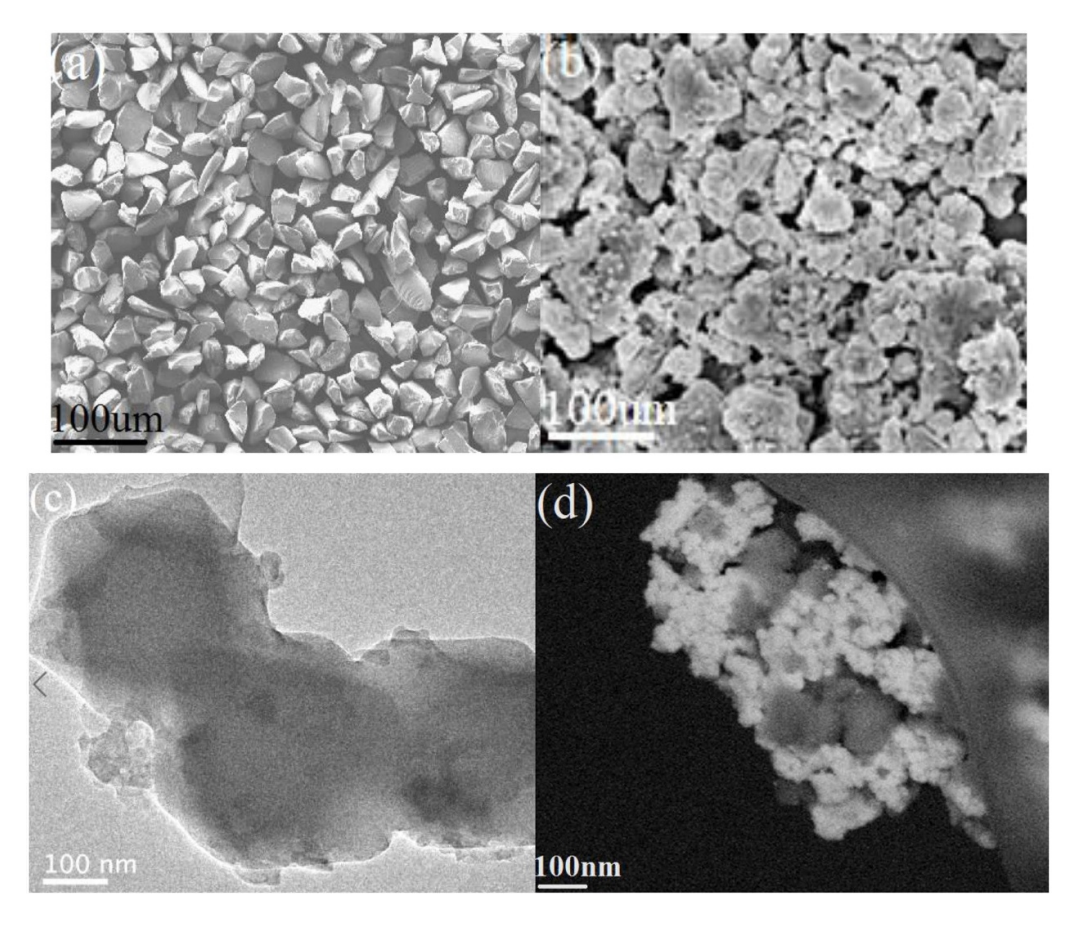


Figure 1. FE-SEM image of commercial Si-thiol (a) and Pd/Si-thiol catalyst (b); TEM image of commercial Si-thiol (c) and Pd/Si-thiol catalyst (d).

the Si-thiol particles ranging from 10 s to 100 s of μm with irregular shapes and the smooth surface and particle edge can be clearly identified. After the incorporation of Pd, the Si-thiol support breaks into smaller and porous particles with rough surfaces and the particles tend to interconnect with each other as shown in figure 1(b), resulting from the mixing and soaking in the organic solution. The above phenomenon can be further distinguished by the TEM images as demonstrated in figures 1(c) and (d) for commercial Si-thiol and Pd/Si-thiol catalyst, respectively.

Figure 2(a) shows a bright field (BF) TEM image of Pd/Sithiol catalyst and the dark spots with diameters less than 5 nm are the uniformly dispersed Pd particles or clusters in the matrix of the modified silica, resulting from the thermal decomposition of Pd(OAc)₂ [14]. The high-angle annular dark-field (HAADF) STEM technique was employed to investigate the Pd deposits since the HAADF image is formed by incoherent electron scattering and is sensitive to heavy elements with the scattering cross-section roughly proportional to the squared atomic number Z^2 of the scattering element [15]. Figure 2(b) shows the HAADF-STEM image (not in the same area as figure 2(a)) and the white spots associated with Pd species could be clearly identified as evenly distributed on the support. Figure 2(c) shows a typical high-resolution HR-TEM image and the lattice fringes of 0.225 nm in dashed white circle correspond to the 111 planes of the Pd crystal. A large number of Pd deposits appeared typically as clusters of few atoms as exhibited in the figure 2(d) where the dashed white circles indicate non-crystalline Pd clusters. x-ray energy dispersive spectroscopy (EDS) analysis confirmed the sample of Pd/Sithiol consisted of Si, O, C, S and Pd (figure 2(e)).

Aberration-corrected (AC) STEM-HAADF imaging suggested that the Pd nanoparticles in various regions under examination were typically less than 5 nm in diameter, as shown in figure 3. Individual Pd atoms (white squares), Pd clusters with few atoms (white circles) and Pd nanoparticles of a few nanometers (dashed outlines) were detected. It was estimated from AC-STEM that the individual Pd atoms, Pd atom clusters and Pd nanoparticles roughly accounted for about 20%, 70% and 10%, respectively, of the particles seen in aberrationcorrected STEM images. Generally, when the thickness of projected specimen was adequately small, STEM-HAADF revealed highly localized area with the electron beam focused around 0.1 nm in diameter [16]. Moreover, the HAADF images represent a projection of atoms or features along the incident beam direction, thus surface atoms cannot readily be distinguished from the subsurface atoms. Pennycook et al used AC STEM-HAADF to determine the location of Pd atoms in carbon fibers by changing the focus of electron beam to obtain images sequentially with the through-the-focus operation [17]. However, the depth location of the Pd atoms in the Si-thiol matrix in current work could not be easily identified

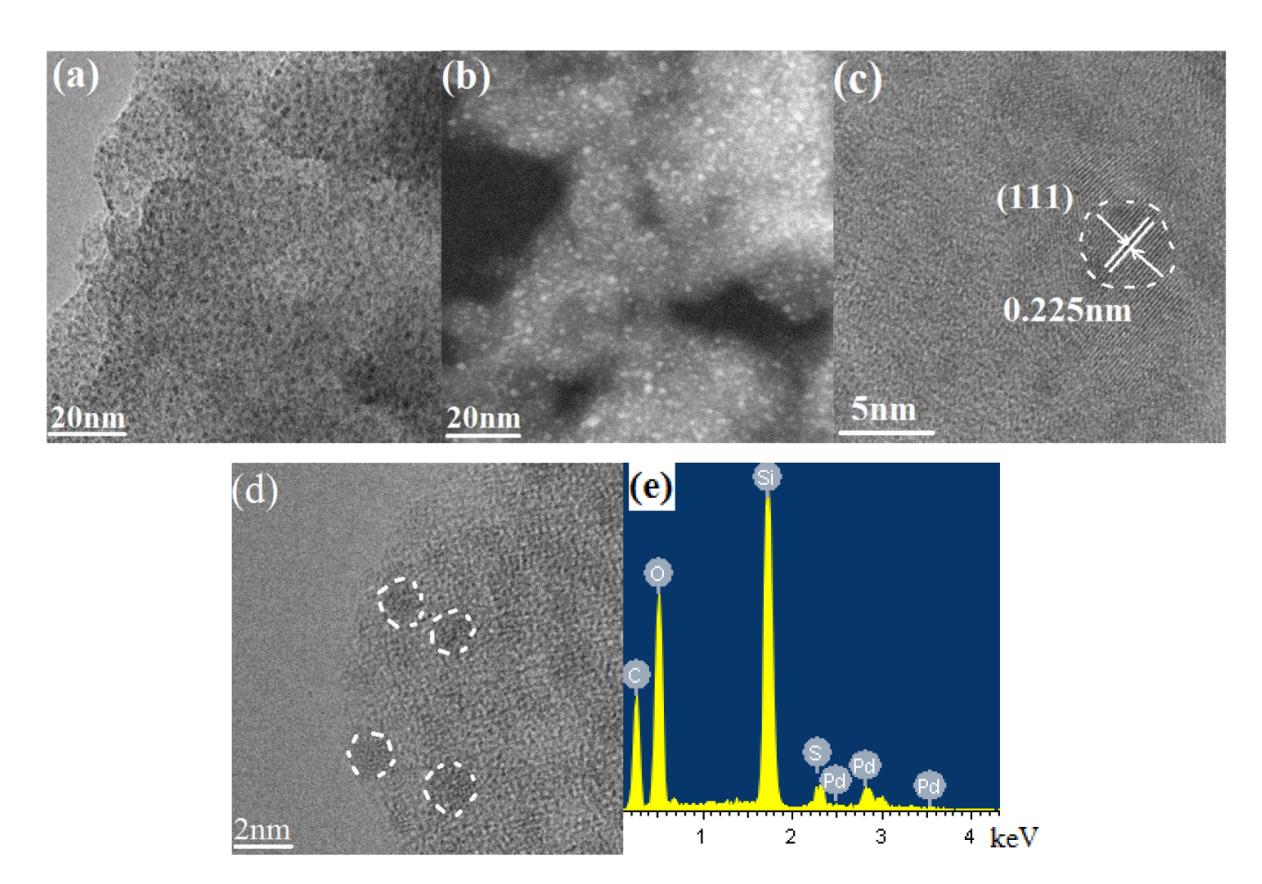


Figure 2. BF-TEM (a), STEM -HAADF (b), HRTEM for nanoparticle (c), HRTEM for nanoclusters (d), and EDS (e) of Pd/Si-thiol catalyst.

by the same method since the Si-thiol contains much more complicated elements as revealed by EDS and the thickness is much thicker than graphene substrates used in Pennycook's work. Therefore, in-situ observation and imaging by varying the specimen exposure time to electron beam were utilized to obtain additional insight into the property of Pd species. From figures 3(b)-(f), the nanoparticle (noted as 1) did not significantly change under the electron beam exposure, suggesting that it was highly stable. The white areas of atom clusters were also largely stable except that a minority of clusters tended to aggregate (noted as 4, 5). The components of this hybrid catalyst system appear to be able to maintain a thermodynamic and/or kinetic steady state in 300 keV electron beam environment. Those Pd atoms trapped in the volume of the Sithiol matrix remained stable during image acquisition while atoms that are on the surface of the Si-thiol were relatively mobile under the electron beam exposure at a dose rate of about 120 e⁻ Å⁻² per second.

3.2. XRD analysis

Figure 4 shows the XRD patterns of Si-thiol matrix and Pd/Si-thiol. As expected, Si-thiol appears relatively amorphous with a single broad peak near 22 degrees, similar to that of SiO₂. The Pd/Si-thiol curve did not reveal evidence for the Pd crystalline phase because of the limited quantity and high dispersion of atomic Pd clusters in the Si-thiol matrix [18]. This result is consistent with the AC-STEM analysis that the Pd nanocrystal accounts for about 3% by volume, and Pd exists

as highly dispersed atom clusters anchored in the amorphous Si-thiol matrix.

3.3. FT-IR analysis

Figure 5 shows the FT-IR spectra of Si-thiol matrix and the Pd/Si-thiol catalyst. The band at 3451 cm⁻¹ corresponds to Si–OH stretching vibration. The band at 2926 cm⁻¹ was attributed to the –OH bending vibration of adsorbed water. The band at 1096 cm⁻¹ confirmed the presence of S–H bonds. The band at 466 cm⁻¹ was due to the bending vibrations of Si–S bonds. Compared with the Si-thiol matrix, a new adsorption peak at 1632 cm⁻¹ could be identified corresponding to the absorption peak of Pd–O–Si bond [19], implying that the Pd species were indeed anchored in Si-thiol support via metal-O-substrate bonds, which may further lead to individual Pd atoms and clusters.

3.4. XPS analysis

XPS analysis was employed to investigate the surface chemical compositions and the valence states of species. Figure 6(a) is an XPS survey spectrum of Pd/Si-thiol, in which Si, Pd, O, C and S peaks were observed, consistent with the EDS results. The Pd 3d spectrum of Pd/Si-thiol is shown in figure 6(b). The binding energy of the Pd 3d5/2 located at 336 eV was assigned to the isolated Pd(0) species and the binding energy at 337.45 eV corresponded to Pd–O–Si [20], indicating part of Pd atoms are immobilized on Si-thiol, consistent with the

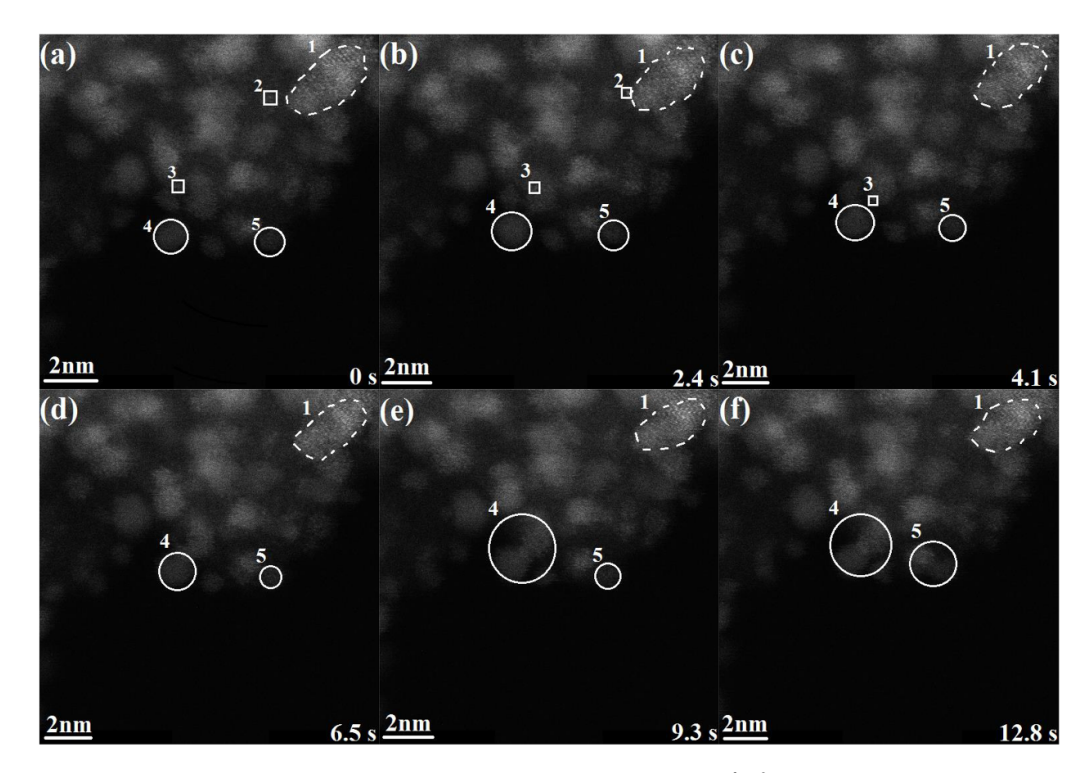


Figure 3. In-situ time sequence of high-resolution STEM-HAADF (dose rate \sim 120 e - Å⁻² s) of Pd/Si-thiol exposed to electron beam (a) \sim 0 s; (b) 2.4 s; (c) 4.1 s; (d) 6.5 s; (e) 9.3 s; (f) 12.8 s, dashed circle represents nanoparticle, white circle represents atom clusters and white square represents single atom, respectively.

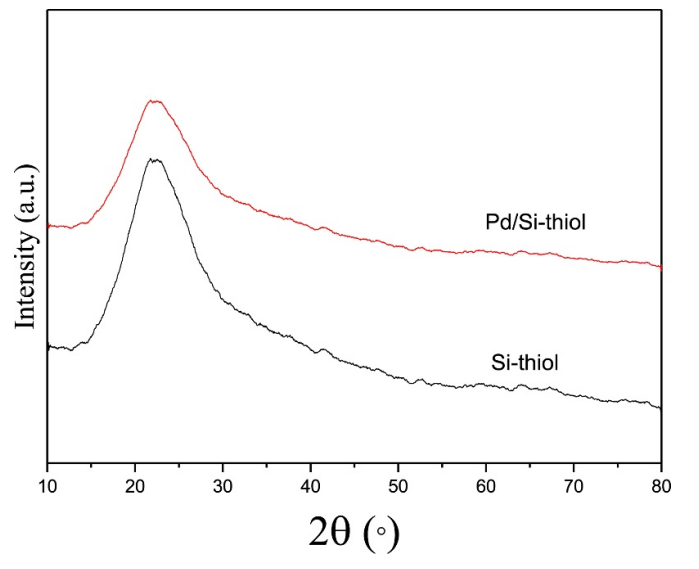
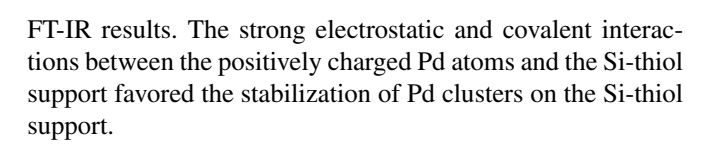


Figure 4. XRD pattern of Si-thiol matrix and Pd/Si-thiol.



3.5. Formation mechanism of Pd/Si-thiol catalyst

In the present preparation, $Pd(OAc)_2$ was chosen as the precursor due to the fact that it has stronger affinity to the

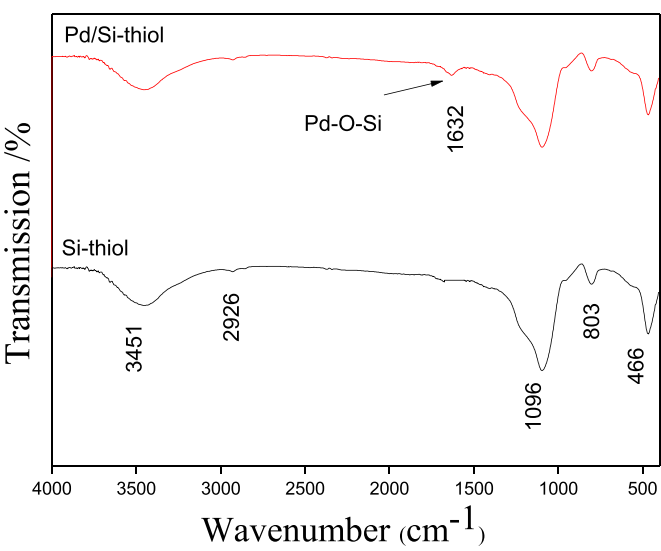


Figure 5. FT-IR spectrum of Si-thiol and Pd/Si-thiol.

thiol-based absorbent than Pd(0) sources, which favors the cross-coupling reactions at ambient temperature. A schematic diagram of the formation mechanism is shown in figure 7. By heating with Si-thiol in toluene (equation 1), the Pd ions were effectively absorbed into Si-thiol scaffold and reduced to Pd(0) atoms in the presence of toluene. This phenomenon was also evidenced by the filtrate becoming colorless and the remaining solid turning brownish. The Si-thiol matrix acted as a source as well as a sink of single atoms and clusters. In Adrio's work, the fast generation of catalytically active Pd(0) species was

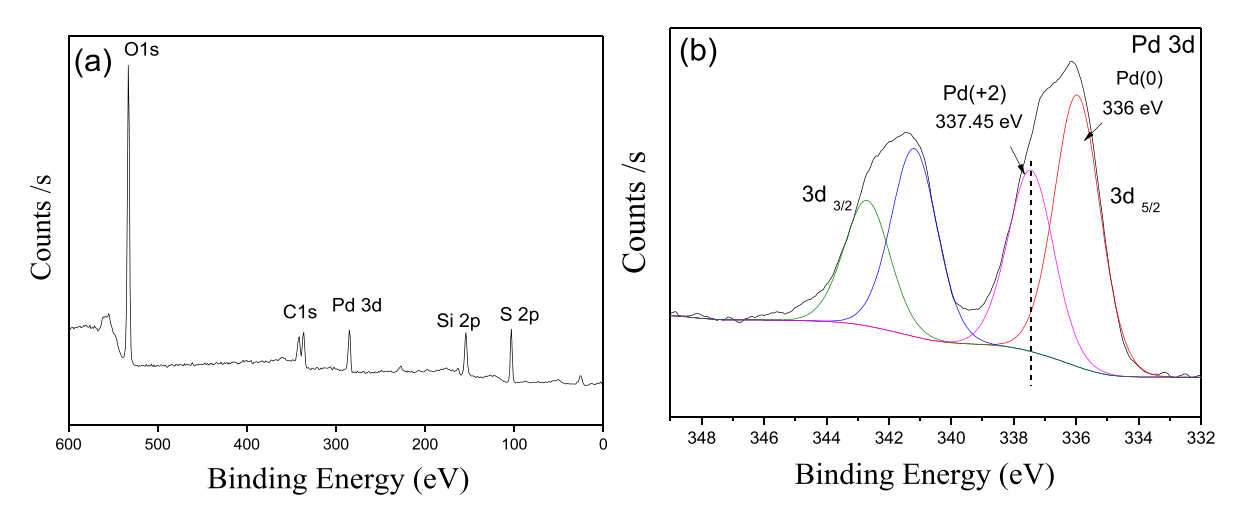


Figure 6. XPS spectrum of Pd/Si-thiol, (a) survey scan, (b) Pd 3d.

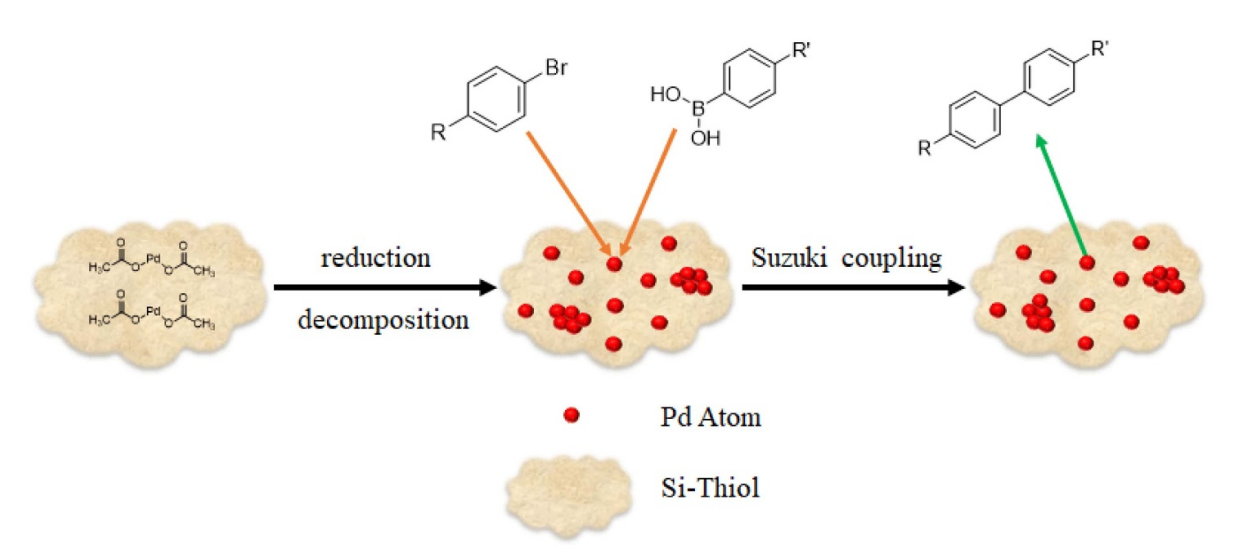


Figure 7. Schematic formation of Pd/Si-thiol catalyst.

counter-acted by an equally rapid Pd aggregation, leading to the premature catalyst deactivation [14]. In the present work, the Pd atoms had a strong tendency to aggregate with others to form clusters. However, most of them could be isolated due to the anchoring sites in Si-thiols, which is different from Adrio's report. Notably, atoms which were not immobilized may further nucleate and grow to form abnormally larger particles that may deactivate the catalyst [21, 22].

3.6. Kinetics of the Suzuki coupling reaction

Previous studies have demonstrated that individual Pd(0) atoms were of much higher catalyst activity than Pd nanoparticles. This is in agreement with Qian's results in which higher catalytic activity was observed for smaller Pd(0) nanoparticles in the Suzuki reaction [23]. The major catalytic deactivation pathway appears to be the aggregation of Pd to form large nanoparticles.

In this work, the Pd/Si-thiol was used as catalyst in Suzuki reaction. p-anisole bromide was reacted with

p-trifluoro-methyl-benezene boronic acid (equation 2) in a variety of solvents at 85 °C (or respective refluxing temperatures if lower). Through extensive analysis of various Pd loading including Pd(OAc)₂/Si-thiol = 1/4 (A), 1/2 (B), and 1/1 (C), the catalytic activity of 1/4 Pd Si⁻¹-thiol ratio was found to be much slower while the performances of 1/2 and 1/1 Pd loadings were comparable, suggesting that the atomic-scale Pd species, single atoms and clusters, immobilized on the Si-thiol indeed play significant role in the Suzuki reaction. Therefore, the 1/2 loading (B) was adopted for further study.

A comparison of kinetics of the coupling reaction determined in different solvents is shown in table 1. The solvents had a drastic influence on the outcome of the reaction. There was no reaction at all in DMF after 22 h of heating (entry 1a), while a moderate yield of 58% was obtained with 1/10 of water added (entry 1b), and the 1/1 mixture of DMF/water gave a much lower conversion of only 34% (entry 1c). The same trend was observed with toluene that adding water does not improve the reaction quite as much (entries 2a–2c). A better result of 86% was achieved in dioxane while the yield decreased to 30%

Table 1. Suzuki coupling between *p*-anisole bromide and *p*-CF₃-benzene boronic acid.

$$\label{eq:meometric} \text{MeO-} \begin{picture}(100,0) \put(0,0){\mathbb{Z}} \put(0,0){$$

Entry	Solvent	Solvent/water	Time (h)	Yield (%)
1a	DMF		22	0
1b	DMF	10/1	20	58
1c	DMF	1/1	30	34
2a	Toluene		19	4
2b	Toluene	10/1	20	88
2c	Toluene	1/1	21	48
3a	Dioxane		32	86
3b	Dioxane	10/1	16	30
3c	Dioxane	1/1	16	95
4a	THF		24	28
4b	THF	10/1	24	26
4c	THF	2/1	24	22
5a	MeCN		24	24
5b	MeCN	10/1	24	20
5c	MeCN	2/1	24	15
6a	MeOH		40	33
6b	MeOH	2/1	24	30
7a	EtOH		18	94
7b	EtOH	10/1	40	86
7c	EtOH	1/1	40	91
8a	n-PrOH		8	96
8b	n-PrOH	10/1	20	85
8c	n-PrOH	2/1	13	95

Table 2. Suzuki coupling between aryl bromides and aryl boronic acids.

$$MeO - CF_3 \xrightarrow{\text{Pd/Si-Thiol}} MeO - CF_3 \xrightarrow{\text{CF}_3} (3)$$

Entry	R	R'	Time (h)	Yield (%)
1a	MeO	Н	3	99
1b	MeO	OMe	20	96
1c	MeO	CO_2H	24	77
1d	MeO	CO_2Et	3	94
2a	Me	Н	1	96
2b	Ac	Н	1	99
2c	CN	Н	1	99
2d	CHO	Н	1	98
2e	CO_2H	Н	5	80
3a	Me	OMe	6.5	85
3b	Ac	OMe	1	99
3c	CN	OMe	1	98
3d	CHO	OMe	2.5	92
4a	Ac	CF ₃	2	93
4b	Ac	CF ₃	2	98
4c	Ac	CF ₃	2	99

when 1/10 of water is added. The 1/1 mixture of dioxane and water gave a high yield of 95% (entry 3a–3c). Reactions in THF, MeCN and MeOH were rather sluggish and they did not benefit from the addition of water either (entries 4a–6b). Reactions in alcohols with higher boiling temperatures gave satisfactory results (entries 7a–8c). Typically, good yields of

>90% were observed in ethanol and propanol. Despite that adding 1/10 of water decreased the conversions (entries 7b and 8b), the 1/1 or 2/1 mixture of alcohols and water only slightly decreased the reaction kinetics.

Moreover, we examined the Suzuki reactions between various aryl bromides and aryl boronic acids (equation 3) using

the as-obtained catalyst. As shown in table 2, good to high yields were obtained for a variety of *para*-substituted substrates. With benzene boronic acid as a coupling partner, the reactions proceeded rapidly to give yields of >95% within 1–3 h (entries 1a, and 2a–2d). The electron-deficient substitutions on aryl bromides also had beneficial effects on reaction times (entries 2b–2e, and 3b–3d).

By using p-acetophenyl bromide and p-CF₃-benzene boronic acid as coupling partners, the recyclability of Pd/Sithiol was evaluated. The first run reached a 93% yield within 2 h, and the second and third runs gave even slightly better results (entries 4a-4c). XPS characterization of the Pd/Sithiol catalyst recycled for three times was performed and no significant differences were detectable from those of the as-synthesized catalyst. Figure S1 (available online at stacks.iop.org/Nano/31/355704/mmedia) exhibits an example of the XPS results, suggesting the oxidation state of Pd/Si-thiol is not changed after the release and recapture of Pd species in Suzuki reaction, consistent with the findings reported by López et al in a relevant but different system [8]. HRTEM and STEM images of the used catalyst (shown in figure S2) reveal very little agglomeration of the Pd atom clusters and nanostructures after the catalytic reactions, implying the recyclability of Pd/Si-thiol catalyst is stable. Additional XRD and FT-IR analyses did not reveal appreciable differences, either, between the as-synthesized catalysts and after repeated uses for three times. In addition, the catalyst separation was much easier due to the fact that the encapsulated Pd atoms were already immobilized in the matrix [24]. These characteristics demonstrate that the present hybrid catalyst composite is efficient, reusable and easily controllable.

4. Conclusions

Pd/Si-thiol catalysts were prepared by decomposing Pd(OAc)₂ in a commercial Si-thiol substrate to form uniformly dispersed Pd atoms, clusters and nanoparticles. The active Pd species were predominantly individual Pd atoms and atom clusters which are strongly tethered in porous Si-thiol matrix. Suzuki reaction revealed that the catalytic activity of the catalyst system had a great dependence on the choice of solvent. The reactions were slow in DMF and did not improve much by adding water, while the use of n-propanol gave the best results. Recycling of Pd/Si-thiol was achieved over three runs without noticeable loss of activity. Since the most effective use of supported metal catalysts is to downsize the metal nanostructures to well-dispersed and atomically distributed active centers, i.e. single-atom catalysts or an ultimate dispersion of catalytic metals, ongoing work aims at optimizing the preparation condition to obtain single-atom Pd/Si-thiol catalyst in combination with DFT modeling to explore the feasibility of a hybrid catalyst system for Heck coupling and Sonogashira coupling.

Acknowledgments

This project was partially supported by UD DBI CAT program, the US National Science Foundation EPSCoR

Grant (IIA-1301765) and National Science Foundation of China (51674043). YZ and CN gratefully acknowledge partial support from the II-VI Foundation. DCM acknowledges partial support from the National Science Foundation DMR-1808048, The authors are grateful to Dr Andrew Herzing at the National Institute of Standards and Technology for his help with the aberration-corrected STEM-HAADF characterization.

Conflicts of interest

There are no conflicts of interest to declare.

ORCID iD

Xiazhang Li https://orcid.org/0000-0002-2528-4121

References

- [1] Miyaura N and Suzuki A 1995 Chem. Rev. 95 2457-83
- [2] Qi L, Zhou X, Li X, Li W, Lv M and Guo M 2015 Appl. Organomet. Chem. 29 244–6
- [3] Lang R et al 2019 Nat. Commun. 10 234
- [4] Webb J D, MacQuarrie S, McEleney K and Crudden C M 2007 J. Catal. 252 97–109
- [5] Nohair B, MacQuarrie S, Crudden C M and Kaliaguine S 2008 J. Phys. Chem. C 112 6065–72
- [6] Minakata S and Komatsu M 2009 Chem. Rev. 109 711–24
- [7] Walcarius A, Etienne M and Lebeau B 2003 Chem. Mater. 15 2161–73
- [8] López M, Esquivel D, Jiménez-Sanchidrián C, Voort P and Romero-Salguero F 2020 Materials 13 623
- [9] Fusini G, Rizzo F, Angelici G, Pitzalis E, Evangelisti C and Carpita A 2020 Catalysts 10 330
- [10] Wang J, Liu C, Kan X, Wu X, Kana J and Dong Y 2020 Green Chem. 22 1150
- [11] Davis J and Hanyu Y 2010 Nanotechnology 21 265302
- [12] Shao X, Yang X, Xu J, Liu S, Miao S, Liu X, Su X, Duan H, Huang Y and Zhang T 2019 Chem 5 693–705
- [13] Ding G, Hao L, Xu H, Wang L, Chen J, Li T, Tu X and Zhang Q 2020 Comm Chem 3 43
- [14] Adrio L A, Nguyen B N, Guilera G, Livingston A G and Hii K K 2012 Catal. Sci. Technol. 2 316–23
- [15] Li T T, Bogle S N and Abelson J R 2014 Microsc. Microanal. 20 1605–18
- [16] Majert S and Kohl H 2015 *Ultramicroscopy* 148 81–86
- [17] Benthem K, Bonifacio C S, Contescu C I, Gallego N C and Pennycook S J 2011 Carbon 49 4059–63
- [18] Andersen H L and Christensen M 2015 Nanoscale 7 3481–90
- [19] Li L, Zhao J, Yang J, Fu T, Xue N, Peng L, Guo X and Ding W 2015 RSC Adv. 5 4766–9
- [20] Zhu G, Fujimoto K, Zemlyanov D Y, Datye A K and Ribeiro F H 2004 *J Catal.* 225 170–8
- [21] Qiao B, Wang A, Yang X, Allard L F, Jiang Z, Cui Y, Liu J, Li J and Zhang T 2011 Nat. Chem. 22 634
- [22] Lin J, Wang A, Qiao B, Liu X, Yang X, Wang X, Liang J, Li J, Liu J and Zhang T 2013 J. Am. Chem. Soc. 135 15314-7
- [23] Qian D J, Wakayama T, Nakamura C and Miyake J 2003 J. Phys. Chem. B 107 3333–5
- [24] Peters B and Scott S L 2015 J. Chem. Phys. 142 104708